$$E_{CT} \times [organic\ C] + E_{AC} \times [abs.\ C] + E_{FS} \times [soil] + E_{CM} \times [coarse\ mass] \quad (5.8)$$

The efficiencies are defined the same as those in Equation 5.7. E_{AC} is the absorption efficiency for light absorbing carbon.

5.2 Preliminary Data Analysis

Before attempting the estimation of light extinction efficiencies and budgets with WHITEX data, some preliminary analyses of the data were performed. These included (1) an investigation of extinction coefficients measured by the transmissometer compared to scattering coefficients measured by the integrating nephelometer for the full range of relative humidity conditions; and (2) comparisons of the results of several analyses using the extinction and scattering coefficients and particulate matter concentrations for separate carbon and nitrate data sets. These were used to examine whether use of light extinction data could help resolve the discrepancies between collocated measurements of carbon and nitrate and perhaps illuminate which data sets would be more appropriate to use in subsequent analyses, including estimation of extinction efficiencies and budgets. Refer to Chapter 3 for more discussion of the carbon and nitrate measurements.

5.2.1 Optical Data and Relative Humidity Effects

Historically, most short term and many long term visibility research programs have relied on the integrating nephelometer as the instrument of choice for measuring atmospheric aerosol scattering. Atmospheric extinction was then approximated by estimating the absorption coefficient. Atmospheric absorption is usually determined using the laser integrating plate method (LIPM) or by measuring elemental carbon and assuming a light absorption efficiency. Given the large discrepancies found in this and other studies between elemental carbon measurements and between elemental carbon derived absorption and LIPM, determinations of extinction by these methods are approximate at best.

Fortunately, Page, Canyonlands, and Hopi Point, were each equipped with both a nephelometer and a transmissometer, which measures extinction directly. This allowed intercomparison of the scattering coefficients measured by the nephelometer (b_{scat}) to the extinction coefficients measured by the transmissometer (b_{ext}). Relative humidity (RH) was also monitored at each of these sites. Time traces of these data, as well as the differences between b_{ext} and b_{scat} and the ratios of b_{ext}/b_{scat} are shown in Figures 5.2, 5.3, and 5.4. Note that the largest extinction coefficients occurring during WHITEX were measured at Page during Feb. 11 - 13 (Julian days 42 - 44) when the relative humidity remained above 60 percent for several days.

At Hopi Point and Canyonlands, transmissometer data are often missing when the relative humidity is high. This is a result of the altitudes of these sites (7100 and 5925 feet above mean sea level, respectively) which frequently causes the sight paths to be obscured by clouds on high RH days. The elevation at Page (4180 feet) is apparently low enough so that this did not occur as frequently.

Scatter plots of the ratios of b_{ext}/b_{scat} as a function of relative humidity are shown in Figures 5.5, 5.6, and 5.7 for the three sites. The mean ratios are near unity (1.10, 1.03, and 1.28 for Page, Hopi Point, and Canyonlands, respectively) when the relative humidity is below 60 percent. As discussed above, there are few transmissometer data at Hopi Point and Canyonlands when the relative humidity is higher than this. However, at Page, it can be seen that the ratio increases dramatically as the relative humidity increases from 70 to near 100 percent. It is known that

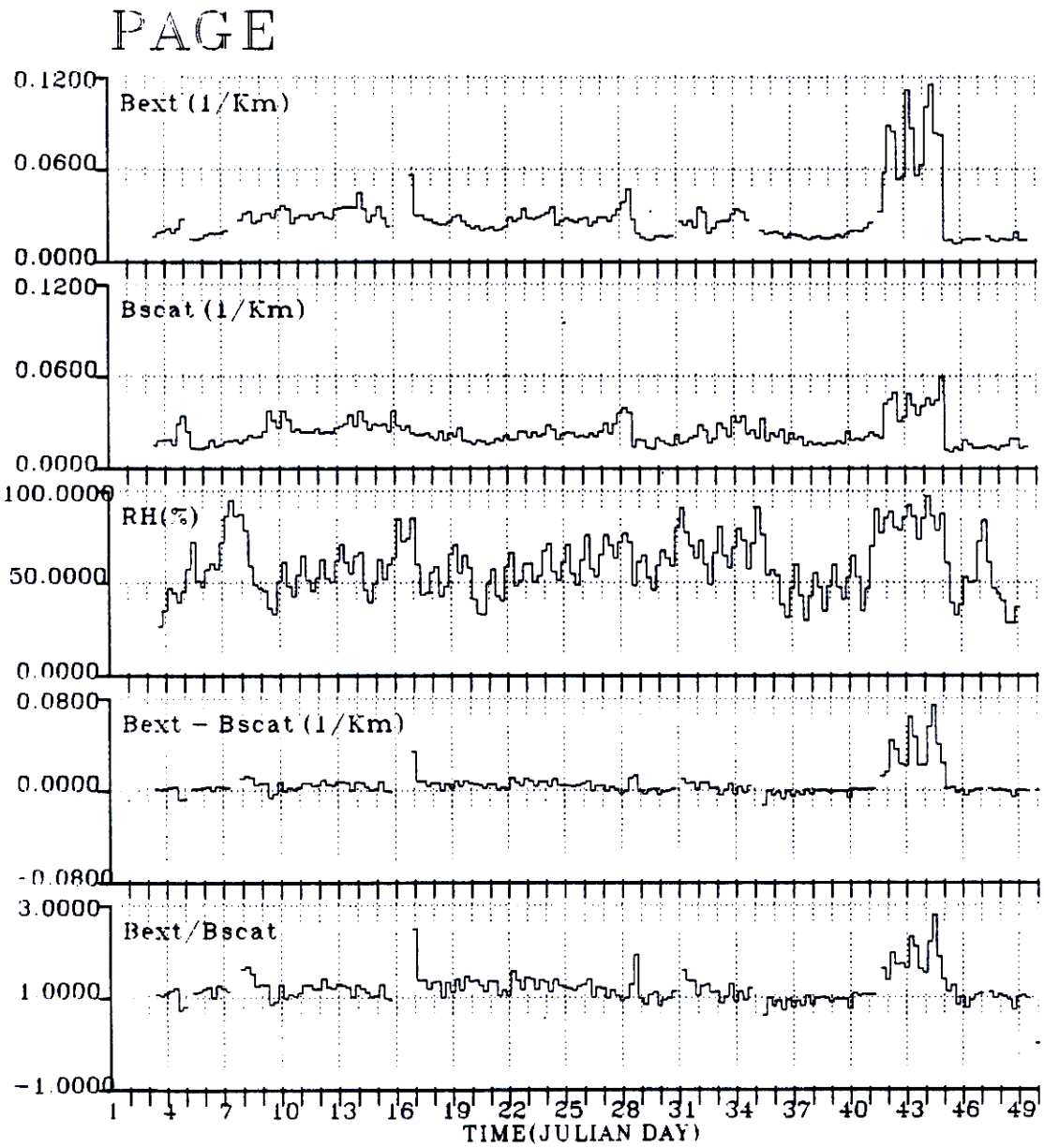

Figure 5.2: Time traces of optical data and relative humidity at Page

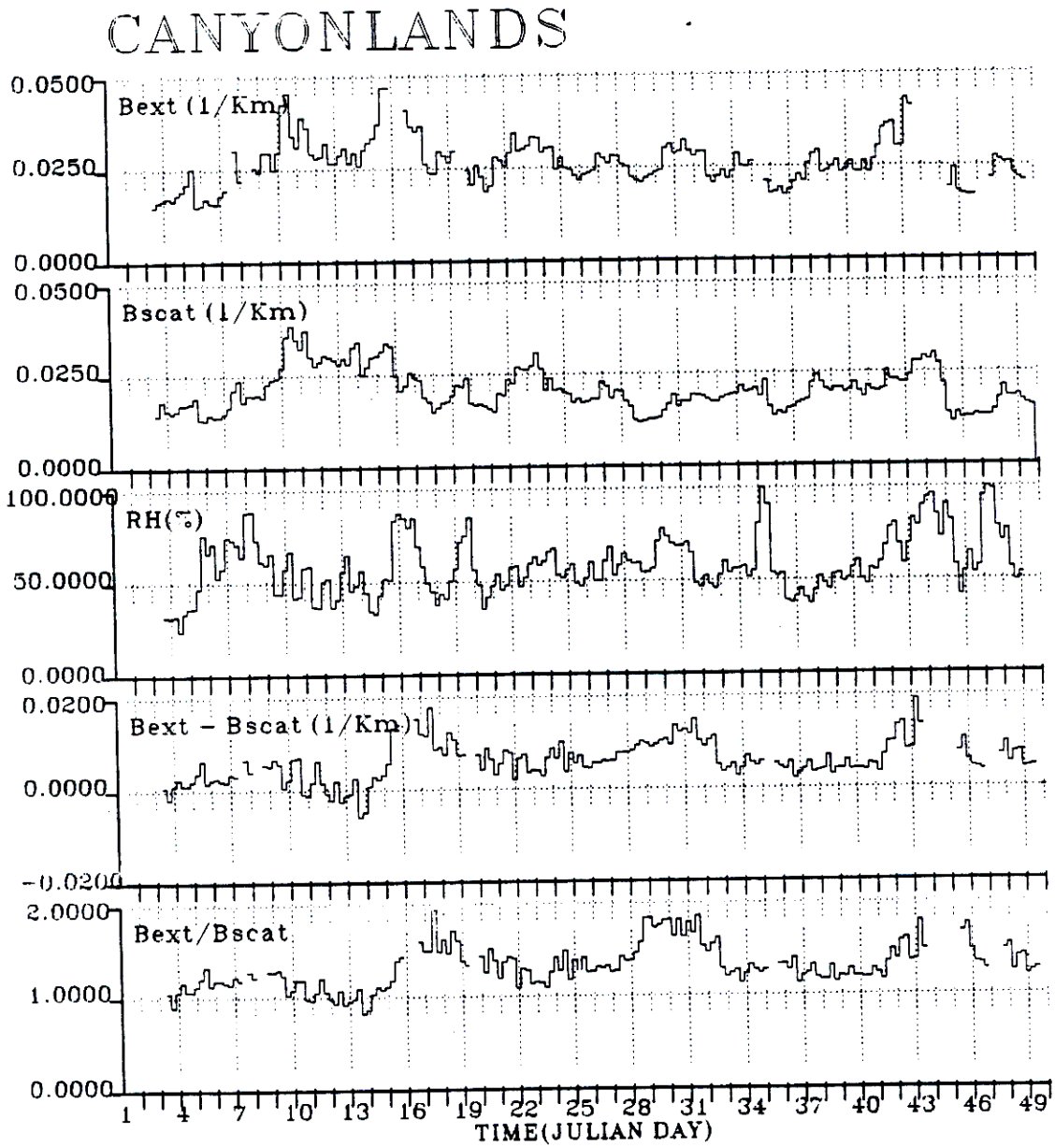

Figure 5.3: Time traces of optical data and relative humidity at Canyonlands.

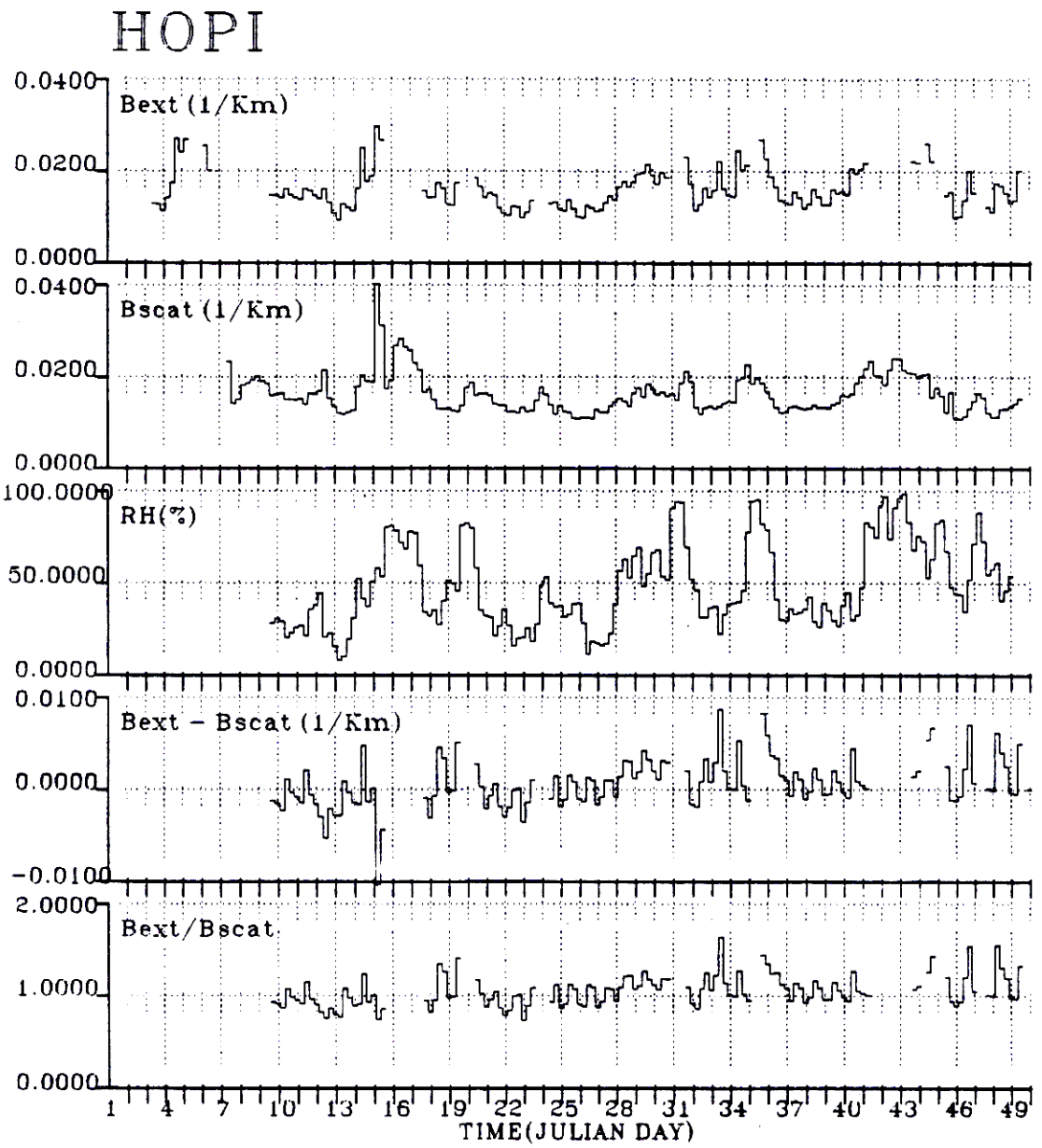

Figure 5.4: Time traces of optical data and relative humidity at Hopi Point.

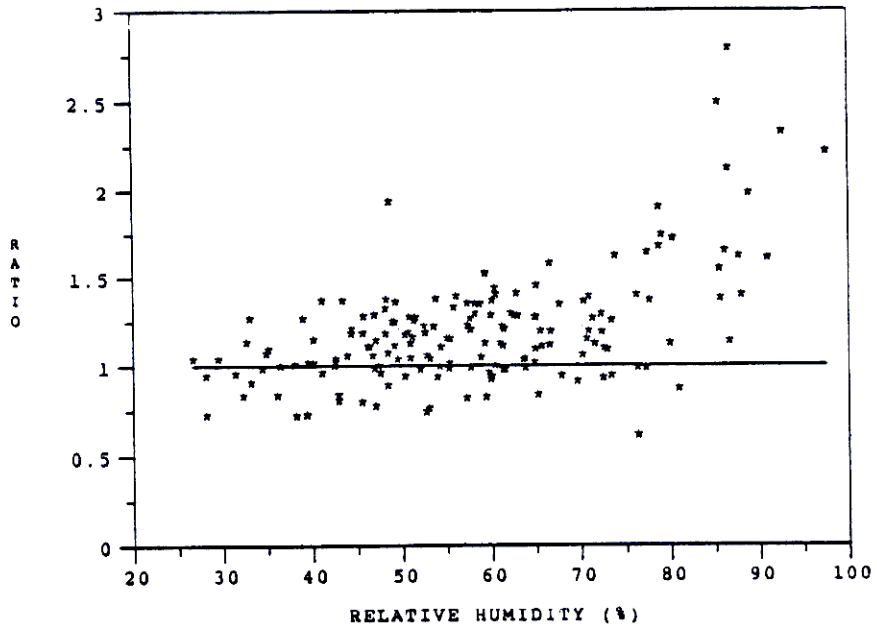

Figure 5.5: Ratio of b_{ext}/b_{scat} as a function of relative humidity for Page.

unmodified nephelometers tend to heat air as it passes through the sampling chamber and, as such, "dry" hygroscopic aerosols, thus reducing their scattering efficiency.[6, 8] Drying the aerosol in the nephelometers used during the WHITEX study appears to cause underestimation of atmospheric scattering by a factor of nearly 3 during high (greater than 90 percent) relative humidity conditions.

Inspection of the time plots for Canyonlands reveals an apparent offset problem between the transmissometer and nephelometer after January 16. The offset is approximately .003-.004 Km^{-1}. To correct for this, in all following analyses, .0035 Km^{-1} was subtracted from all b_{ext} data after January 16 at Canyonlands. Tables 5.10, 5.11, and 5.12 include the means and other statistics for the optical data. The statistics for Canyonlands include the .0035 Km^{-1} correction. Note that mean b_{scat} is greater than mean b_{ext} at Hopi Point. This is probably due to the time periods with high RH when b_{ext} was missing because the transmissometer site path was obscured by clouds but b_{scat} data existed. During many of these time periods, the measured scattering was relatively high. To confirm this "different data set theory", the means of b_{ext} and b_{scat} only for time periods when both measurements were nonmissing were also calculated. The mean b_{ext} for these 127 time periods was .0158 Km^{-1} and the mean b_{scat} was .0151. No corrections were made to this data set.

5.2.2 Examination of Carbon Data

At Page and Hopi Point measurements of carbonaceous material were made by both IMPROVE and SCISAS samplers. Data from the IMPROVE samplers were analysed using the thermal optical reflectance (TOR) method. Data from SCISAS samplers were analysed by the thermal MnO_2 oxidation (TMO) method. As discussed in Chapter 3, the organic carbon concentrations from the two methods agreed fairly well, but the elemental or "light absorbing" carbon, while correlating well, differed by a factor of approximately 5 with the TOR concentrations being greater. Scatter plots and time traces of these data are in the appendices of Chapter 3. Correlation matrices are shown in Tables 5.13 and 5.14.

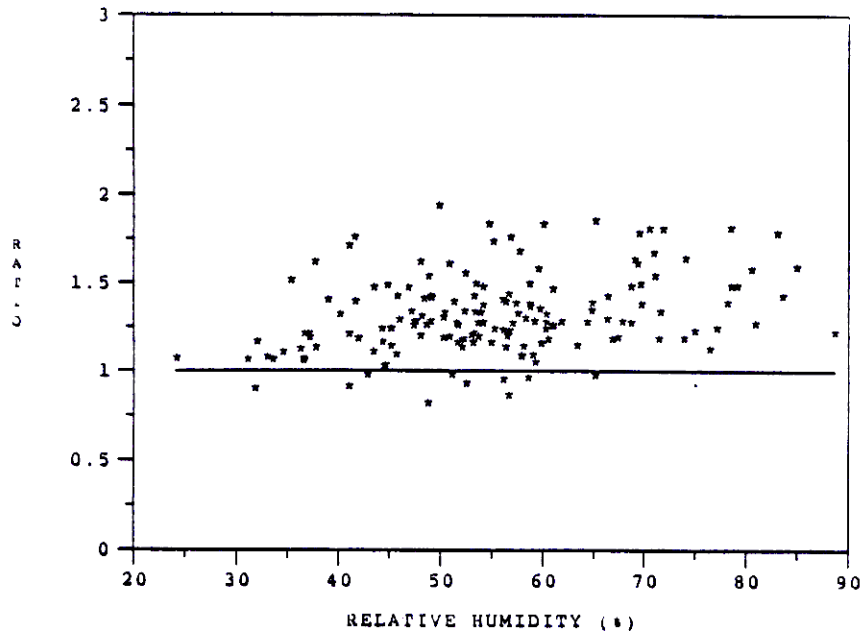

Figure 5.6: Ratio of b_{ext}/b_{scat} as a function of relative humidity for Canyonlands.

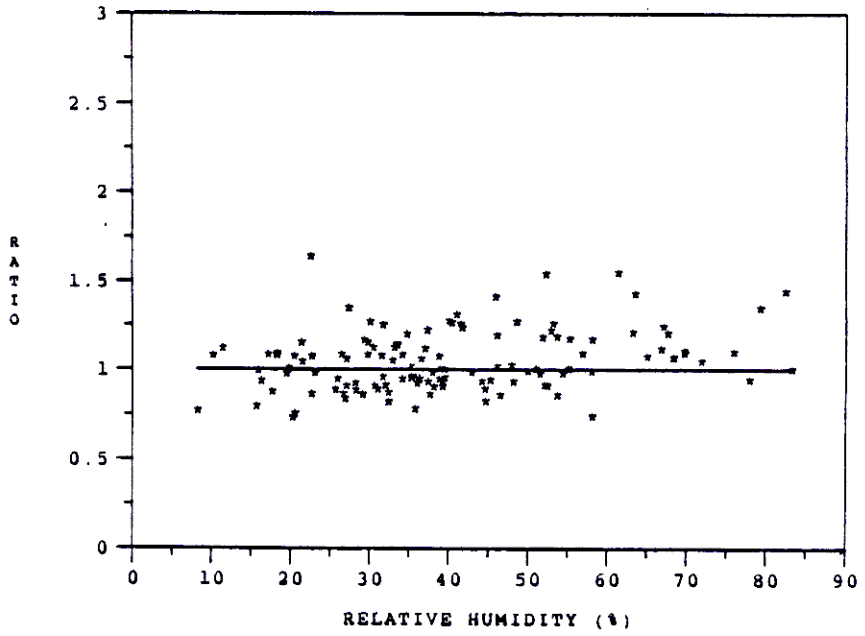

Figure 5.7: Ratio of b_{ext}/b_{scat} as a function of relative humidity for Hopi Point.

Table 5.10: Statistics for the 6-hour averaged optical data at Page (Km^{-1}). The low relative humidity subgroup is defined as RH < 60%.

Page						
Humidity Subgroup	Variable	Mean	Standard Deviation	Minimum	Maximum	Number of Cases
All	b_{ext}	.0283	.0176	.0115	.1158	173
Low	b_{ext}	.0219	.0064	.0115	.0355	102
All	b_{scat}	.0230	.0083	.0108	.0594	185
Low	b_{scat}	.0201	.0054	.0108	.0380	103
All	b_{ext}/b_{scat}	1.19	0.32	0.61	2.78	173
Low	b_{ext}/b_{scat}	1.10	0.20	0.72	1.94	102
All	$b_{ext}-b_{scat}$	.0054	.0114	-.0126	.0742	173
Low	$b_{ext}-b_{scat}$	.0018	.0040	-.0079	.0132	102
All	RH(%)	59.3	15.9	26.6	97.4	182
Low	RH(%)	47.6	8.6	26.6	59.9	100

Table 5.11: Statistics for the 6-hour averaged optical data at Canyonlands (Km^{-1}). The low relative humidity subgroup is defined as RH < 60%.

Canyonlands						
Humidity Subgroup	Variable	Mean	Standard Deviation	Minimum	Maximum	Number of Cases
All	b_{ext}	.0239	.0067	.0133	.0470	165
Low	b_{ext}	.0230	.0063	.0133	.0470	118
All	b_{scat}	.0206	.0057	.0113	.0387	186
Low	b_{scat}	.0205	.0060	.0113	.0387	119
All	b_{ext}/b_{scat}	1.32	0.22	0.82	1.94	165
Low	b_{ext}/b_{scat}	1.28	0.22	0.82	1.94	118
All	$b_{ext}-b_{scat}$	.0059	.0041	-.0059	.0191	165
Low	$b_{ext}-b_{scat}$	.0050	.0037	-.0059	.0178	118
All	RH(%)	58.7	15.7	24.1	100.0	182
Low	RH(%)	49.0	8.0	24.1	59.9	115

Table 5.12: Statistics for the 6-hour averaged optical data at Hopi Point (Km^{-1}). The low relative humidity subgroup is defined as RH < 60%.

Hopi Point						
Humidity Subgroup	Variable	Mean	Standard Deviation	Minimum	Maximum	Number of Cases
All	b_{ext}	.0161	.0044	.0093	.0298	137
Low	b_{ext}	.0155	.0042	.0093	.0298	120
All	b_{scat}	.0162	.0042	.0109	.0402	169
Low	b_{scat}	.0152	.0038	.0109	.0402	123
All	b_{ext}/b_{scat}	1.05	0.17	0.73	1.64	127
Low	b_{ext}/b_{scat}	1.03	0.16	0.73	1.64	110
All	$b_{ext}-b_{scat}$	.0007	.0027	-.0104	.0087	127
Low	$b_{ext}-b_{scat}$	.0003	.0026	-.0104	.0087	110
All	RH(%)	48.4	22.9	8.1	98.8	158
Low	RH(%)	35.8	12.2	8.1	59.3	112

Table 5.13: Correlation matrix for carbonaceous material at Page.

	TOR organic carbon	TOR abs. C	TMO organic carbon	TMO abs. C
TOR organic	1.000			
TOR abs. C	0.695	1.000		
TMO organic	0.651	0.848	1.000	
TMO abs. C	0.470	0.744	0.868	1.000

Table 5.14: Correlation matrix for carbonaceous material at Hopi Point.

	TOR organic carbon	TOR abs. C	TMO organic carbon	TMO abs. C
TOR organic	1.000			
TOR abs. C	0.634	1.000		
TMO organic	0.311	0.501	1.000	
TMO abs. C	0.239	0.423	0.807	1.000

To determine whether TOR or TMO data are more appropriate for use in the extinction budget analyses, three tests of the data were performed. These included 1) calculating reconstructed extinction with both data sets, to see which better reproduced measured light extinction; 2) MLR analyses regressing TOR and TMO carbon against b_{ext} to see if realistic absorption efficiencies would result; and 3) estimating the expected mean light absorbing carbon (LAC) concentrations for each site based on the optical measurements.

Reconstructed Extinction

The first test of the LAC concentrations was to calculate reconstructed light extinction using Equation 5.8 with the consensus literature scattering and absorption efficiencies shown in Table 5.9. The analyses were done using both the Trijonis and Pitchford[13] and the modified Tang[12] scattering efficiencies for nitrates and sulfates. NO_3 concentrations were from IMPROVE module E. $b_{ext,R}$ was calculated both for TOR carbon concentrations, and using TMO carbon. These values were then compared to the measured b_{ext} less Rayleigh scattering. Absorption due to NO_2 was included in the reconstructed extinction when data were available, otherwise it was set to zero. There are no NO_2 data at Hopi Point and NO_2 data at Page are missing for most high extinction days. This could cause $b_{ext,R}$ to be as much as 3% too low at Page for the days when NO_2 was missing. The underestimation would be less at Hopi Point (perhaps 1–2%) since NO_2 concentrations there are probably lower relative to the particulate concentrations than they are at Page.

Results for both Page and Hopi Point are shown in Figures 5.8, 5.9, 5.10, 5.11, 5.12, 5.13, 5.14 and 5.15. They show that at Page, the reconstructed extinction is closer to the measured when TMO carbon is used. The TOR concentrations cause the reconstructed extinction to be too high. However, at Hopi Point, the reverse is true. The TOR carbon concentrations result in reconstructed extinction which is closer to measured. TMO carbon causes reconstructed extinction to be too low. Another observation which can be made is that the 1/(1-RH) correction for sulfates and nitrates is too high. Use of the modified Tang curves eliminates the problem of overestimating the reconstructed extinction during high RH time periods.

Regression Analysis

A second preliminary test of the carbon data was performed by subjecting the data to multiple linear regression (MLR) analyses with b_{ext} as the dependent variable and the chemical species concentrations as the independent variables. The resulting regression coefficients are estimates of the scattering and absorption efficiencies of each species. Use of the absorbing carbon data which are most suitable should then result in an absorption efficiency which is closer to the consensus literature value (9–12 m^2/g).

Three different regressions were done for each site (Hopi Point, Page, and data from the sites combined) and each set of absorbing carbon data (TMO and TOR). Regressions were done using two different sets of independent variables. They were (1) absorbing carbon, other fine mass, and coarse mass for cases when the relative humidity was less than 60 percent and (2) absorbing carbon, sulfates, nitrates, organics, soil, and coarse mass for both the low relative humidity subgroup and for all data. Sulfates and nitrates were corrected for relative humidity effects using the modified Tang curves when data at all humidities were used.

The absorption efficiencies predicted for absorbing carbon by each of these MLR analyses are shown in Table 5.15. At Page, all of the MLR coefficients for TOR absorbing carbon were insignificant ($t > .05$). Use of TMO absorbing carbon at Page resulted in a significant, but negative

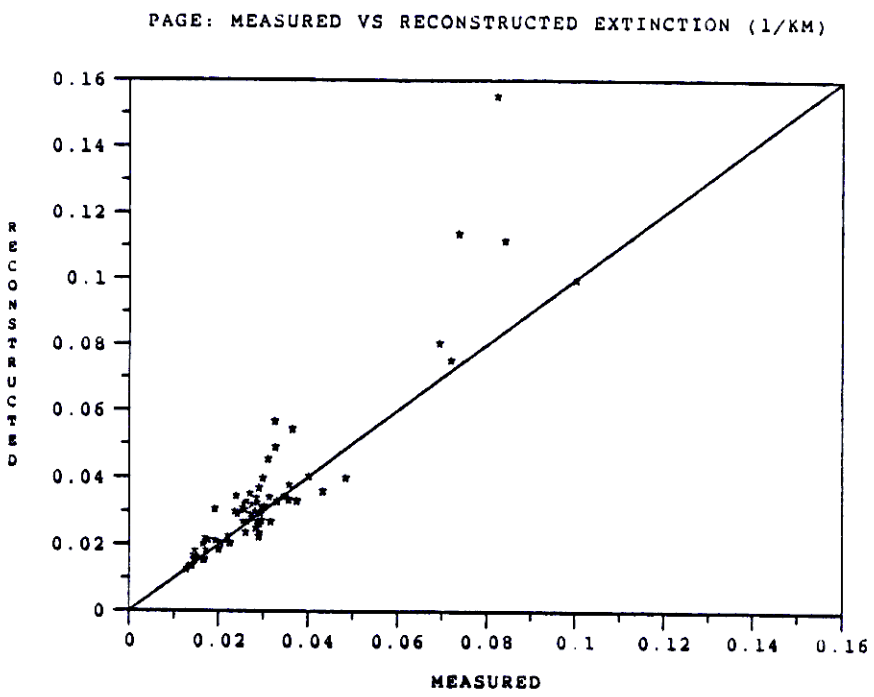

Figure 5.8: Scatter plot of measured extinction vs reconstructed extinction for Page using TMO carbon. Sulfate and nitrate scattering efficiencies are both 2.55/(1-RH).

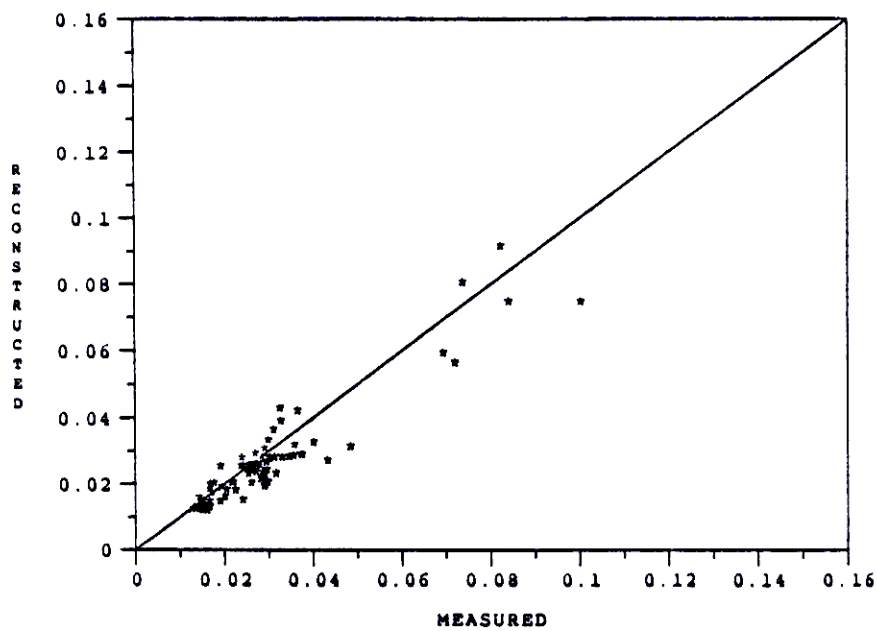

Figure 5.9: Scatter plot of measured extinction vs reconstructed extinction for Page using TMO carbon. Sulfate scattering efficiency is 2.55× fs(RH). Nitrate scattering efficiency is 1.1×fn(RH).

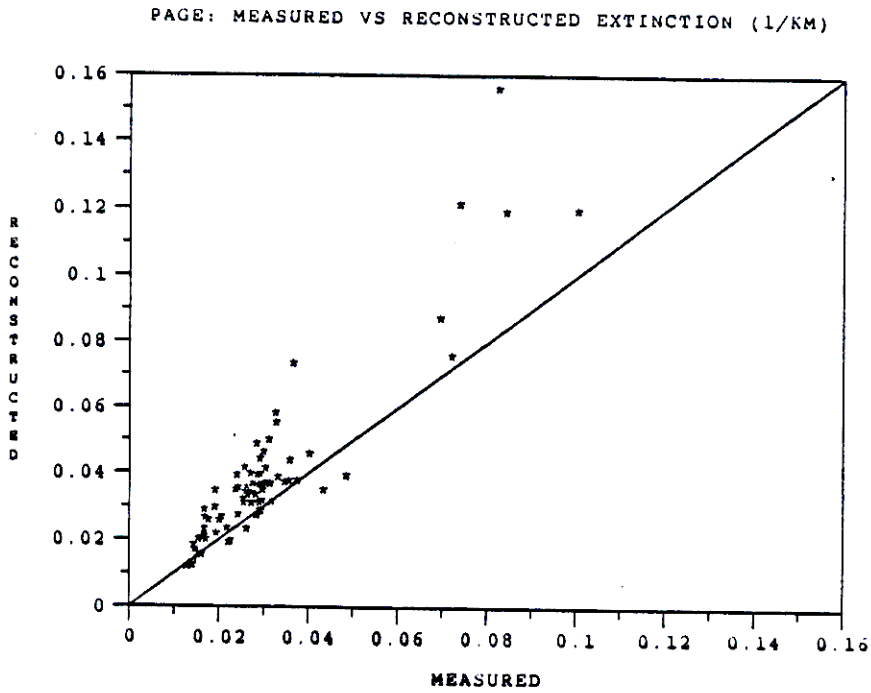

Figure 5.10: Scatter plot of measured extinction vs reconstructed extinction for Page using TOR carbon. Sulfate and nitrate scattering efficiencies are both 2.55/(1-RH).

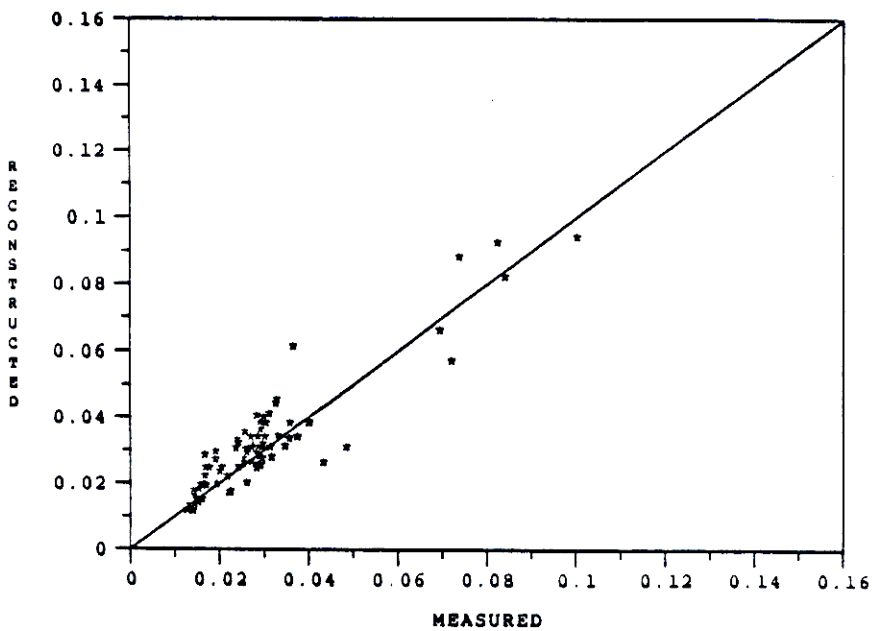

Figure 5.11: Scatter plot of measured extinction vs reconstructed extinction for Page using TOR carbon. Sulfate scattering efficiency is 2.55× fs(RH). Nitrate scattering efficiency is 1.1×fn(RH).

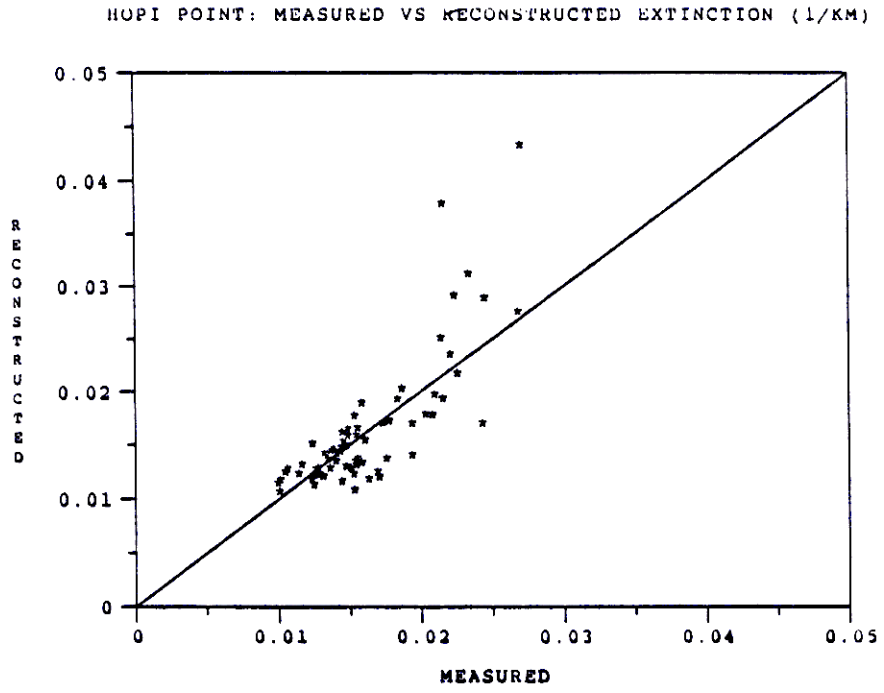

Figure 5.12: Scatter plot of measured extinction vs reconstructed extinction for Hopi Point using TMO carbon. Sulfate and nitrate scattering efficiencies are both 2.55/(1-RH).

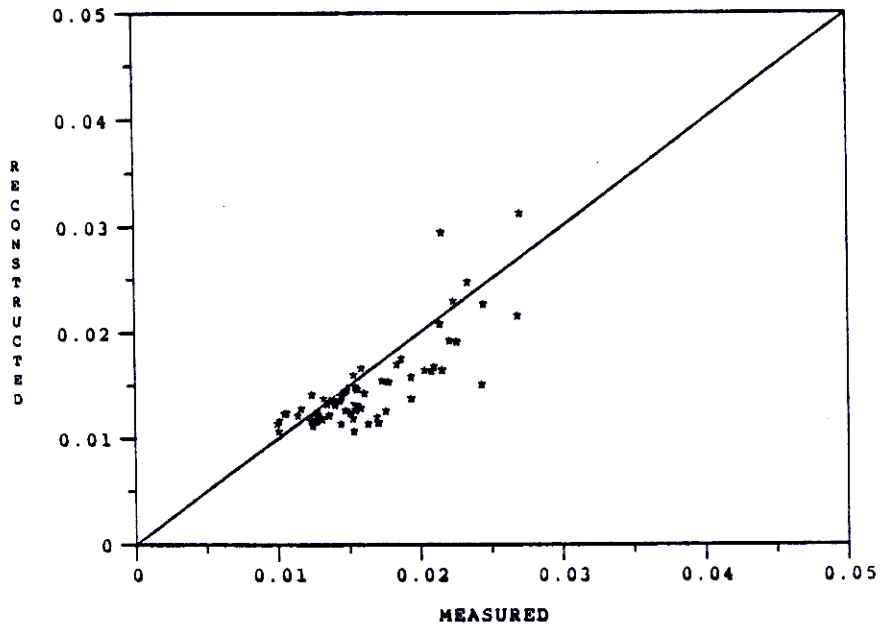

Figure 5.13: Scatter plot of measured extinction vs reconstructed extinction for Hopi Point using TMO carbon. Sulfate scattering efficiency is 2.55× fs(RH). Nitrate scattering efficiency is 1.1×fn(RH).

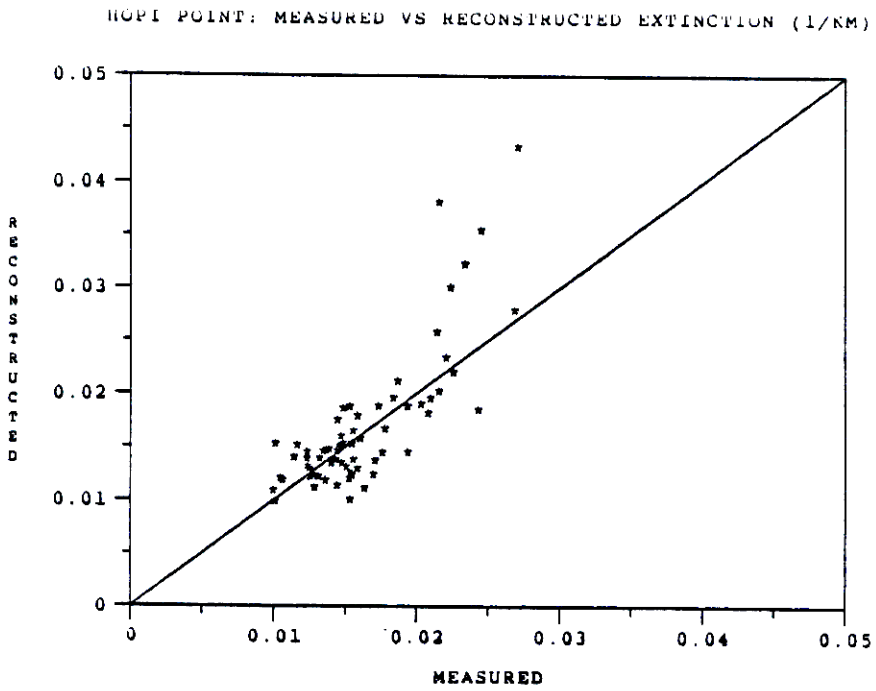

Figure 5.14: Scatter plot of measured extinction vs reconstructed extinction for Hopi Point using TOR carbon. Sulfate and nitrate scattering efficiencies are both 2.55/(1-RH).

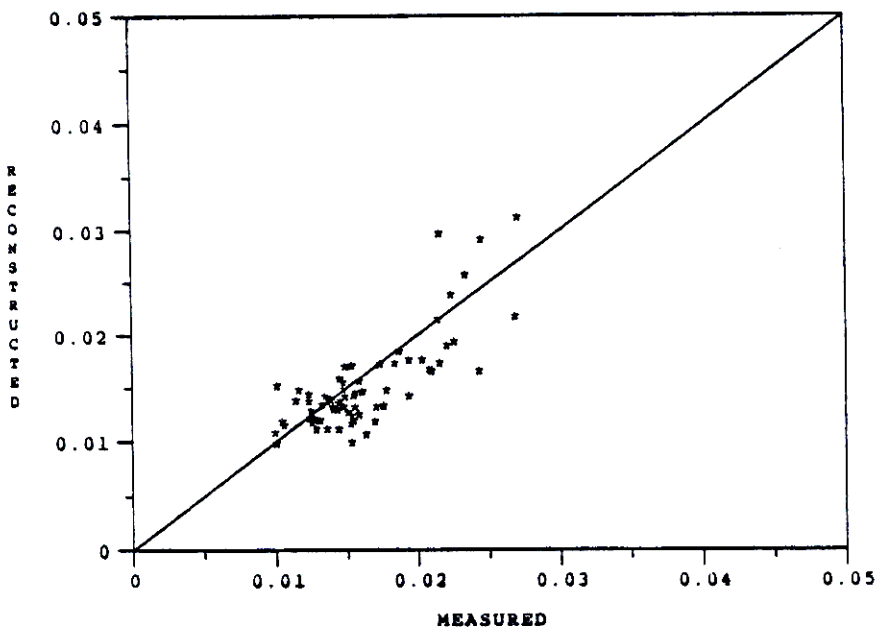

Figure 5.15: Scatter plot of measured extinction vs reconstructed extinction for Hopi Point using TOR carbon. Sulfate scattering efficiency is 2.55× fs(RH). Nitrate scattering efficiency is 1.1×fn(RH).

Table 5.15: Summary of multiple linear regression analyses using TOR and TMO Carbon. Results are the predicted light absorption efficiencies for absorbing carbon ± the standard error in m^2/g. The dependent variable for all analyses was b_{ext}. Low RH refers to RH < 60%.

Site	Independent Variables	RH Subgroup	Results for TOR Carbon	Results for TMO Carbon
Page	all species	All	*-1.6±3.7	-82.0±30.4
Page	all species	Low	*-2.0±4.3	*-57.9±28.0
Page	abs. C, other, coarse	Low	*4.1±3.6	*-28.3±26.7
Hopi	all species	All	11.7±3.8	*-59.9±47.0
Hopi	all species	Low	*6.6±4.7	*-54.9±58.7
Hopi	abs C., other, coarse	Low	13.8±4.3	*-70.4±58.0
Both	abs. C.,other, coarse	Low	8.9±2.5	*21.52±18.0
All	abs C., other	Low	8.2±2.2	No data at Cany

*These values are statistically insignificant (t > 0.05).

efficiency with a large magnitude for one case and insignificant coefficients for the other two cases. Results for Hopi Point, when TOR carbon was used, were in the range of expected values, ranging from 6.6 to 13.8 m^2/g, although one case was insignificant. When TMO carbon was used for Hopi Point, all resulting coefficients were insignificant. Regressions using data from Page and Hopi Point combined, and for Page, Hopi Point, and Canyonlands combined resulted in significant and reasonable coefficients for TOR carbon, and an insignificant coefficient for TMO carbon.

The negative results may be physically reasonable because the presence of light absorbing carbon can reduce light extinction due to chemical or physical interactions between the carbon and other aerosol constituents.[9] One scenario in which additional carbon could reduce light scattering is by changing the particle size distribution. If the aerosol particles consist of insoluble carbonaceous cores with hygroscopic ammonium sulfate coatings then the particles would tend to be larger if the carbon concentration was lower. Assuming the same ammonium sulfate concentration, more carbon means there are more nuclei available, thus the aerosols would be smaller and perhaps scatter less efficiently.

Since the regression coefficients for TOR were more reasonable than the results obtained using TMO carbon, this analysis indicates that the TOR values are more appropriate for use in visibility analyses and that the TMO derived concentrations are underestimates of the light absorbing carbon.

Extinction Derived Absorbing Carbon

One final analysis was done to investigate which of the light absorbing carbon data sets is most suitable. The differences between b_{ext} and b_{scat} when the relative humidity is low should be primarily due to atmospheric absorption. Then the expected absorbing carbon concentrations can be approximated by

$$Absorbing\ Carbon = (b_{ext} - b_{scat})/9.0 \quad RH < 60 \tag{5.9}$$

where 9.0 is the expected absorption efficiency in m^2/g. Since b_{scat} as measured by the nephelometer does not include all of the large particle scattering and hence somewhat underestimates the total scattering, this equation would be expected to overestimate the absorbing carbon concentrations. Another assumption is that all of the absorption is due to carbon. If this is not true, then the

calculation would overestimate light absorbing carbon by an additional, though probably very small, amount.[13]

At Page, the calculation yielded a mean extinction-derived absorbing carbon (with negative values included) of 0.283 $\mu g/m^3$. The means of the TOR and TMO absorbing carbon data for the same time periods are 0.432 and 0.092 $\mu g/m^3$, respectively. At Hopi Point, the extinction derived concentration was 0.039 $\mu g/m^3$, while means of TOR and TMO absorbing carbon are 0.126 and 0.027 $\mu g/m^3$, respectively. Based on this analysis, it appears that the TMO derived absorbing carbon measurements, on average, are too low and TOR concentrations are too high.

Recommendations

Evidence from the three preliminary analyses is inconclusive. The reconstructed extinction analysis shows that using TOR concentrations gives more reasonable results at Hopi Point, but TMO gives better results at Page. Use of multiple linear regression analysis to estimate the absorption efficiency indicates that TOR carbon is more reasonable. And finally, calculation of the mean extinction derived light absorbing carbon shows that TMO carbon is probably too low, while TOR is too high.

Though the preliminary analyses are inconclusive, it was decided that when calculating the WHITEX extinction budgets, TOR carbon concentrations would be used rather than TMO.

5.3 Light Extinction Budget By Extinction Type

For each of the sites for which there are adequate data, light extinction is apportioned into absorption by gases, absorption by particles, scattering due to gases, and scattering by fine and coarse particles.

There are no coarse mass data for Canyonlands and gaseous NO_2 concentrations exist only for Page. Consequently, a full extinction budget by type can be explicitly calculated only for Page. A budget by type for all constituents except absorption by NO_2 is possible for Hopi Point. Since NO_2 concentrations were low at Page and probably lower at all other WHITEX sites, this is not a serious obstacle. Coarse mass scattering as well as gaseous absorption must be estimated for Canyonlands. Time plots of all the relevant particulate and gaseous data for Page, Canyonlands, and Hopi Point are shown in Figures 5.16, 5.17, and 5.18. Statistics for the same data are shown in Tables 5.16, 5.17, and 5.18.

To generate the extinction budgets by type for each site, the mean extinction coefficients for each extinction type were estimated independently. The details of these calculations are discussed in the following subsections. Not unexpectedly, the sums of the components do not exactly equal the means of the measured extinction coefficients. The fractions of light extinction allocated to each component are determined by dividing the estimated mean coefficient for each type by the sum of the means for all types. Rayleigh scattering is included in the total. Table 5.19 summarizes the extinction budgets by type for each of the three sites. The budgets for the three sites are also illustrated by the pie charts shown in Figure 5.3.

5.3.1 Scattering by gases (Rayleigh Scattering)

Scattering of light by air molecules is referred to as Rayleigh scattering. The amount of Rayleigh scattering or "clean" air scattering is dependent on the wavelength of the light and on the density of air molecules. Assuming that air density depends mostly on altitude, the average Rayleigh